2019 EAGE ANNUAL
81ST CONFERENCE + EXHIBITION
LONDON | THE UNITED KINGDOM

Tu_P02_14

Time-Lapse Elastic Properties of Cracked Granite During Deformation Inferred from Laboratory Experiments Using 2-D Waveform Modelling

S. Lai[1]*, N. Fuji[1], I. Katayama[2]

[1] Institut de Physique du Globe de Paris; [2] Hiroshima University

Summary

In order to understand the physics of earthquake generation, we study the microscopic weakening process in a centimetre-scale laboratory experiment. A series of deformation experiment was performed to the granite sample from Aji region, Japan. During the experiments, active seismic wave propagation was measured. This study numerically models the observed waveform in order to infer to the time-lapse elastic structure changes.
We first modify the finite difference code on collocated Cartesian introducing zig-zag free-surface discontinuities. We applied response function estimation to the synthetic waveform to consider all the effect (i.e. 3-D effect, instrumental response, attenuation). We use trial-and-error method to find the best-fit velocity models using full waveform synthetics with response. Then we use the same method to make a series of velocity models for the automated Monte Carlo scheme. Comparing automated velocity models using different methods, we find that L1 norm is the best fitting method. We further tested fault models that we find the trend of the changes of the velocity model after the creation and during the thickening of the fault. This method will detail a microscopic weakening process during the nucleation of earthquakes using full waveforms, which have an impact on fundamental understanding of earthquake physics.

Introduction

Full waveform analysis of active data during deformation experiments could provide more localised 2-D details than those based only on travel time measurements. The detailed time-lapse 2-D images will lead to new insights into microscopic dynamics during weakening and rupture processes. In order to constrain the physics of the weakening and rupture processes of initially unfractured rock in a laboratory scale, and to better understand the earthquake nucleation, we perform waveform modelling to infer to the time-lapse elastic structure changes during laboratory experiments focusing on full waveform details.

Many studies intend to start from finding general physical characteristics from laboratory experimental data. Lockner et al. [1977] obtained the changes of seismic velocity models and attenuation during the deformation by calculating the traveltime. Zaima and Katayama [2018] applied triaxial deformation experiment on a centimetric-scale granite from Aji region, Japan, under dry and wet condition. They found that as an axial pressure applied on the top of the sample increases and the rock sample deforms gradually, the time-lapse data obtained from the receiver show the trend of the velocity change. However, from Lockner et al. [1977] to Zaima and Katayama [2018], they only used P- and S-wave traveltimes picked only for one station, providing averaged wavespeeds of the rock with little knowledge on the temporal stress distribution changes. These waveforms can provide us more information on structural changes than only velocity changing. Thus, in this study, we used the experimental data of Zaima and Katayama [2018] and full-waveform modelling to match the observed waveforms to obtain the velocity models and the waveforms changes during the deformation of the rock. We build a series of velocity models with response estimation and implement an automatic Monte Carlo waveform fitting method to obtain the best-fit velocity models. In addition, we also performed many tests for lateral heterogeneity. We have tried random models, fault models, etc., to successfully simulate the different distributions of wavefields and the waveforms. From these results, we can construct a rough process of weakening of the rock sample to help understanding the physical characteristics of the earthquake nucleation.

Method and Theory

In order to calculate elastic wavefield in a medium with a curve discontinuities or free surface boundaries, we can use a tensorial formulation of the wave equation and curvilinear coordinate transformations to make the computational uniform grid coincide with the curved interface in physical domain (e.g. Komatitsch and Tromp [1999]). We used finite-difference on collocated Cartesian introducing zig-zag free-surface discontinuities. However, we modified the boundary conditions for optimally accurate collocated finite-difference method based on predictor-corrector scheme (Takeuchi and Geller [2000], Fuji et al. [2016]) for 2-D P-SV medium in this study.

We tried to perform the modelling in the same geometry and conditions as the experiments. The parameters used are dt=0.002 μs, dx=0.005 cm, and dz=0.005 cm. The source wavelet is sent as the real input source used in the experiments with 2 MHz resonant frequency in compressional and shear axes. Since the source is on the side of the cylinder, we put the point source on the top and put one receiver at the bottom of the 2-D circle (Fig. 1A). Here we can use the reciprocity theorem to model synthetic waveforms for the sources of two kinds: compressional and shear, just by using a single force from the receiver to the antipode source position and calculate the compressional and shear strains. We start with homogeneous model since the Aji granite is reported to be nearly isotropic texture with a small compressional wave anisotropy (< 1.3%) and shear wave velocity has no significant changes in different polarisation directions. Homogeneous velocity models are tested in different P-wave and S-wave velocities in order to find a best-fit model for the experimental waveform results during the deformation.

Numerical Examples

We take the velocity model from Zaima and Katayama [2018], comparing it with the observed waveform. It obviously shows the shortcomings of using hand-picking method with only first arrival to infer to the velocity models. We use full waveform for data fitting instead. However, the waveform misfit is too large to go beyond the first arrival fitting for the moment and thus we further explored the way to better model the waveforms.

There are many reasons that will cause the differences between synthetics and observed data. In our case of 2-D circle disk forward modelling, 3-D effect, instrumental response, attenuation, finite-surface source, and other unknowns, may cause a huge discrepancy between observed and synthetic data. Hence, we design the response function estimation, which involves all the impact factors into the function, in order to rebuild the similar synthetics to the observed waveform. Since we have:

$$\mathcal{F}^{-1}\left[\frac{\mathcal{F}(u_{\mathbf{m}1}^{obs})(t)}{\mathcal{F}(u_{\mathbf{m}1}^{syn})(t)}\cdot\mathcal{F}(u_{\mathbf{m}1}^{syn}(t))\right]=u_{\mathbf{m}1}^{obs}(t) \quad (1)$$

we can have the response of the experiment by taking the relationship between the observed waveform and the synthetic waveform of the same model (**m**1). Even though the time-lapse P-wave velocity can be slightly changed due to the first setting of P-wave velocity (**m**1), it will not be as slow as Vp based on hand-picked traveltimes and we value more about the ΔVp but not the absolute Vp in this study. Then, we can get the response function R(ω) as follows:

$$\mathcal{R}(\omega)=\mathcal{F}(u_{\mathbf{m}1}^{obs})(t)\cdot\frac{1}{\mathcal{F}(u_{\mathbf{m}1}^{syn})(t)} \quad (2)$$

We can rebuild the waveform similar to the experimental results from only using the numerical synthetics by doing convolution with the response function:

$$\mathcal{R}(t)*u_{\mathbf{m}2}^{syn}(t)\cong u_{\mathbf{m}2}^{obs}(t) \quad (3)$$

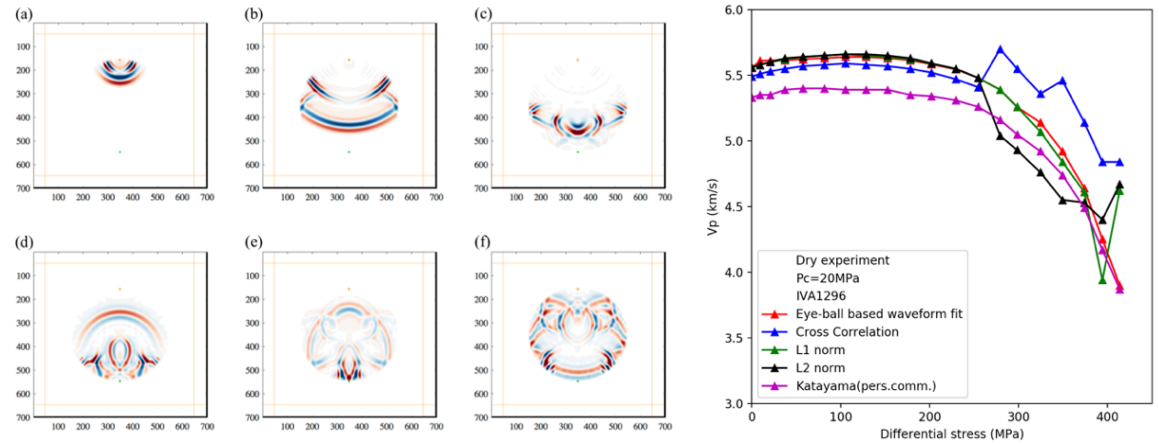


Figure 1 *(A)The time-lapse Z-component wavefield of displacement snapshots. The orange cross denotes the source and the green square denotes the receiver. t=(a) 1.4 ,(b) 3.4 ,(c) 5.4 ,(d) 7.4 ,(e) 9.4,(f) 12.4 μs. (B) Numerical modelled P-wave velocities as functions of the differential stresses of dry sample iva1296 using hand-picking and auto-fitting.*

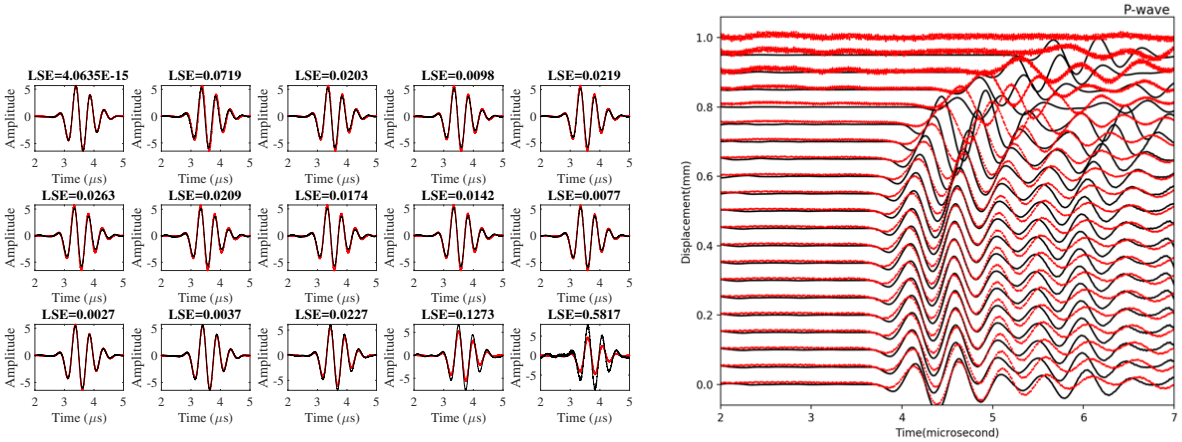


Figure 2 *(A) The rebuilt waveform from 3 to 6 microseconds using the relationship between the observed data and the first synthetic waveform. The error between the observed data and the rebuilt synthetics is calculated by Least Square Error (LSE) method. (B) Observed waveform data plots in red dots and the synthetics with response in black with the new velocities in this study cut from 2 microseconds to 7 microseconds without S-wave arrivals.*

We test several norms to automatically and accurately detect the time-lapse structure changes (Fig. 1B). Therefore, we first comply with the eyeball-based trial-and-error method in order to find the best values of velocity models. We then introduce automated Monte-Carlo methods, which are based on waveform misfit, to construct a system for finding the models fast and accurately. We processed a series of velocity with an interval of $\Delta v = 10$ m/s that we have 191 velocity models for autofitting. The automated Monte-Carlo system will chose the synthetic waveform with the smallest error relative to the observed waveform, and chose this model of synthetic data as the best model.

In order that the synthetic waveforms be comparable to observed data, we use a response function (Eq. 3) that contains all the information other than the structural information that we would like to extract (Fig. 2A). The response function is taken from the relation between the zero-displacement (zero-time-lapse) waveform traces of observed data and synthetics. We truncate the waveforms before shear waves around in from 3 to 6 microseconds, and use it for response function. Applying the same response function to all the waveforms we have, we can obtain the synthetic waveform with the proper transfer function (Fig. 2B).

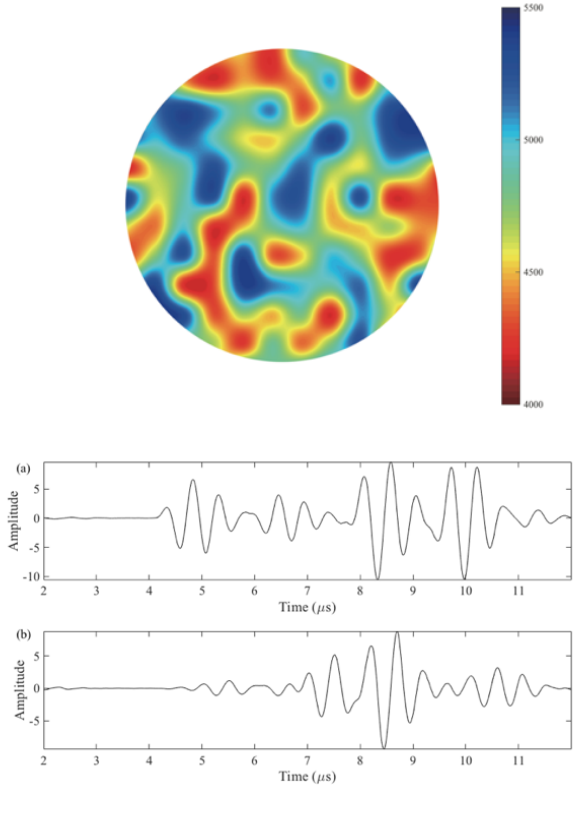


Figure 3 *(A) Random media test with the target circle and colourbar for P-wave velocity from 5500 m/s to 4000 m/s, S-wave velocity 3450 m/s to 2450 m/s, and density ρ in the range of 2500 to 2000. The place outside the circle will be set to zeros when modelling. (B) The synthetic waveform of random media applied with response function. (a) P-wave component (b) S-wave component.*

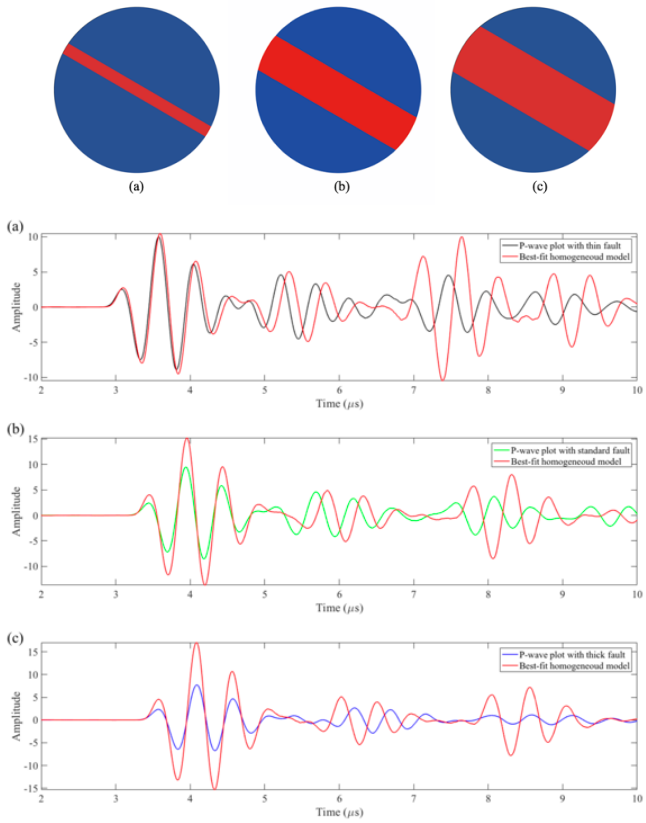


Figure 4 *(A) Models with different width of faults. The surrounding media is 5000 m/s for P-wave velocity and 3124 m/s for S-wave velocity. The fault zone area is 1000 m/s for P-wave velocity and 624 m/s for S-wave velocity. (B) The waveform of the three models with faults in different width and their besi-fit homogeneous waveform. (a) Waveform of the media with thin*

In order to be able to investigate the effect of heterogeneities on the waveforms, we perform random heterogeneous media (Fig. 3). After many tests for random heterogeneous media, we are convinced that it must be able to help a lot with understanding the structure of the sample during the deformation. For the purpose of modelling the wave propagating with a fault inside the media (Fig. 4), we created the

average media with a fault in it with different width to see the waveform changes during the fault development. We perform both the eye-ball based trial-and-error and L1 norm automated Monte-Carlo fitting to find the best-fit homogeneous velocity models for the three fault models. We superimpose the synthetic waveform for homogeneous models on that of fault models to see the difference. In Fig. 4B, we can see the different feature of the waveforms of the fault models to the homogeneous model that we are convinced that the full waveform can give a clue to the structure inside the sample.

Conclusions

We developed the full-waveform-based elastic imaging methods for laboratory rock experiments. We used a finite-difference code on collocated Cartesian coordinate with zig-zag free-surface discontinuities for boundary for the 2-D circle forward modelling. After comparison, we know that the response function estimation can successfully rebuild the waveform before the attenuation influences by considering all the effects, such as 3-D effect, instrumental response, attenuation and etc. After testing, we obtained the best automated fitting method– L1 norm. With response function and eyeball-based waveform fitting and automated Monte-Carlo waveform fitting, we obtained the averaged time-lapse P-wave velocities based on observed waveforms.

In faults modelling test, we know that the existence and extension of faults will lead to the decreasing of the velocity models. The systematic changes in elastic wave velocities in Aji granite during triaxial deformation experiment under dry and wet conditions are related to the development and closure of cracks. In the early stages of deformation, both Vp and Vs increase slightly due to the closure of pre-existing cracks that are mostly oriented normal to the direction of maximum compression stress. Elastic wave velocities then decrease as the sample approaches failure, due to the growth of cracks aligned subparallel to the axis of compression. From the confirmation of real data fitting and faults modelling in this study, we can tell that with the wave propagation information and waveform fitting technique, the physical characteristics of the earthquake generation can be inferred. Using full waveforms, this project will further detail a microscopic weakening process during the nucleation of earthquakes.

The large discrepancy between observed waveform and synthetic before convolution with response function showed that it is necessary to take account for more realistic configuration and to design the laboratory experiments by changing the size of the sample, experimental geometry, and etc. Only by extending the study to the 3-D dimension can we understand the weaknesses and rupturing that may occur in real conditions. We look forward to using this method, the new laboratory experiment design, combined with the finite-element method, to perfectly model the actual situation of the earthquake nucleation and learn about the physical characteristics of the earthquake.

References

Fuji, N., Ovcharenko, O., Martin, R. and Cuvilliez, C. [2016]. Simple and accurate operators based on taylor expansion for 2D elastic seismogram calculation under geological discontinuities with regular cartesian grids. *78th EAGE Conference and Exhibition*, *EAGE Extended abstract*, 05.

Komatitsch, D. and Tromp, J. [1999]. Introduction to the spectral element method for three-dimensional seismic wave propagation. *Geophysical Journal International*, 139(3):806–822.

Lockner, D. A., Walsh, J. B. and Byerlee J. D. [1977] Changes in seismic velocity and attenuation. during deformation of granite. *Journal of Geophysical Research*, 82(33):5374–5378.

Saenger, E. H., Gold, N. and Shapiro, S. A. [2000]. Modeling the propagation of elastic waves using a modified finite-difference grid. *Wave Motion,* 31(1):77–92.

Takeuchi, N. and Geller, R. J. [2000]. Optimally accurate second order time-domain finite difference. scheme for computing synthetic seismograms in 2-D and 3-D media. *Physics of the Earth and Planetary Interiors*, 119(1):99–131.

Virieux, J. [1986]. P-SV wave propagation in heterogeneous media: Velocity-stress finite-difference. method. *Geophysics*, 51(4):889–901.

Zaima, K. and Katayama, I. [2018]. Evolution of elastic wave velocities and amplitudes during triaxial deformation of Aji granite under dry and water-saturated conditions. *Journal of Geophysical Research: Solid Earth*, *123*.